Engineering Applications of Artificial Intelligence 133 (2024) 108527

Contents lists available at ScienceDirect

Engineering Applications of Artificial Intelligence

journal homepage: www.elsevier.com/locate/engappai

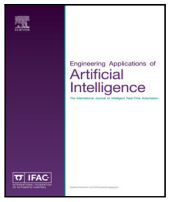

Research paper

Using a generative adversarial network for the inverse design of soft morphing composite beams

Tomaž Brzin, Miha Brojan *

University of Ljubljana, Faculty of Mechanical Engineering, Laboratory for nonlinear mechanics, Aškerčeva 6, Ljubljana, 1000, Slovenia

ARTICLE INFO

Keywords:
Inverse design
Generative adversarial network
Morphing composites
Complex shapes and motions

ABSTRACT

The inverse design of structures having tailored properties is challenging mainly due to the multiple design solutions that can satisfy the prescribed conditions. For example, in the inverse design of morphing composite beams, different fabrication solutions exist because the material, geometry and actuation can be varied. On the other hand, the problem can be highly nonlinear due to the large deformations present in such problems. For this reason, we present a generative adversarial network-based inverse design method for constructing soft composite beams that morph into target shapes and can carry out complex prescribed motions. Our approach makes use of composites with passive and active layers that deform into prescribed shapes due to the strain mismatch induced by the non-homogeneous geometric and material properties as well as temperature actuation. To test the proposed method and explore the parametric space much faster than with heating and cooling, we established a mechanical analog (a toy model) that exploits the mechanical stretching of highly elastic, active layers. Experiments and numerical examples demonstrate the effectiveness of our simple toy model, for which the generator network takes the target shapes as inputs and generates the corresponding design parameters for the fabrication of composite beams that self-deploy into prescribed shapes when released. We extended our method for generating the design parameters for forming soft, morphing composite beams that exhibit complex targeted motions when actuated by temperature. Our data-driven method is simple, yet robust enough to provide solutions to complex problems and aid in the future design of soft robots and smart-deployable structures.

1. Introduction

Morphing structures have the ability to transform from a compacted configuration into deployed forms in which they are stable and can withstand the prescribed loading conditions. They are usually based on the mechanism principle (Holmes, 2019), consisting of rigid links and flexible joints. Another, more advanced approach to structure transformation relies on inhomogeneities of the structure, where stress gradients drive the structure to morph into another configuration (Timoshenko, 1925; van Manen et al., 2018). Recent advances in the design of these structures have attracted many research groups, which studied various mechanisms underlying self-deformation, see, e.g., van Manen et al. (2018), Battista et al. (2019), Caruso et al. (2018), Nojoomi et al. (2021), Pezzulla et al. (2015). However, for this technology to be successfully scaled from research to an industrial level, more robust, inverse-design methods need to be developed first.

There are various ways to induce stress gradients that can activate the self-deployment or spatial transformation of an initially flat or straight structure (van Manen et al., 2018). The shape transformation can be achieved through swelling, which can be activated differently, e.g., by immersion in a solvent bath (Battista et al., 2019; Wu et al., 2019), with temperature (Guo et al., 2013), diffusion (Pezzulla et al., 2015), and light (Wang et al., 2019), but 4D-printed composites that activate their shape-changing with heating and cooling are the most popular among researchers (Ding et al., 2017, 2018; Huo et al., 2022). Another promising example of actuation uses hydrostatic pressure. As shown by Siéfert et al. (2019), a meso-structured elastomer plate can undergo rapid, controllable, and complex shape changes when pressure is applied. The principle of programmable bending can also rely upon an electric field to shape structures made of dielectric liquid-crystal elastomers, see e.g., Qiu et al. (2023). Although the presented mechanisms allow for the fabrication of morphing structures that can achieve different shapes and large deformations, they need an additional external stimulus or activation energy applied during the transformation process, such as pressure, electric field, solvent, temperature or light. On the other hand, self-deployable structures that are made by stacking and bonding together individual, pre-stretched layers store potential

* Corresponding author.
E-mail address: miha.brojan@fs.uni-lj.si (M. Brojan).

https://doi.org/10.1016/j.engappai.2024.108527
Received 5 June 2023; Received in revised form 23 February 2024; Accepted 26 April 2024
Available online 8 May 2024

elastic energy during the fabrication process (van Manen et al., 2018). As a result, these so-called strain-mismatched composites deform from initially flat (2D) configurations to deformed, pre-programmed (3D) forms entirely on their own. They can even be stored and transported in rolled or crumpled configurations and only need to be released when required to deploy into their final forms (Caruso et al., 2018; DeSimone, 2018; Guo et al., 2020; Zavodnik et al., 2023).

To further extend the space of attainable shapes for self-morphing structures, we need to precisely modify the stress-gradient distribution over the initial structural domain. This opens a whole new field of practical applications, such as the development of soft robots and their parts (Ionov, 2015), various self-deployable structures (Pezzulla et al., 2015; Siéfert et al., 2019; Wang et al., 2019), and other biomimetic structures inspired by nature (Nojoomi et al., 2021). As a consequence, a parameter space where multiple solutions exist also greatly expands and thus makes the inverse problem computationally more difficult to solve. To overcome these challenges, different techniques have been proposed. Nojoomi et al. (2021) successfully encoded hydrogel sheets with growth maps using a computational geometry technique to transform them into the target shapes. They experimentally confirmed the success of their algorithm by making small models of cars, fish, and human heads. In the case of origami and kirigami structures that can deploy into target forms, Dang et al. (2022) employed a marching algorithm and Choi et al. (2019) solved the inverse problem with the use of a nonlinear, constrained optimization technique. Machine learning techniques also quickly achieved success. Their attributes are not only used for predicting material properties, designing new materials, and discovering new mechanisms beyond intuition (Guo et al., 2021), but also for empowering evolutionary algorithms to solve inverse problems (Sun et al., 2022; Wu et al., 2020).

A special branch of machine learning, known as generative modeling must be regarded as an important concept in modeling. It is able to generate different independent solutions to the inverse problems in engineering (Regenwetter et al., 2022). For example, Liu et al. (2018) developed a generative adversarial network (GAN) architecture, conditioned by a pre-trained simulator network, to inverse design metasurfaces that exhibit target transmittance spectra. A similar problem was dealt with by Kim et al. (2022), where they expanded the traditional GAN model with a classifier. A conditioned variational autoencoder (VAE) was used in the field of aeronautics for computing supercritical airfoil shapes (Yonekura et al., 2022). Generative models – VAEs (Cang et al., 2018; Ma et al., 2023) and GANs (Kim et al., 2020; Mao et al., 2020) – are also very popular for the design of complex materials with target properties, as they are able to generate new designs of essentially arbitrary patterns. A deep generative model was even used to design bar mechanisms with prescribed trajectories (Kapsalyamov et al., 2023). GAN-based frameworks therefore represent powerful tools for solving inverse problems and can overcome the difficulties when searching across wide parameter spaces, common in nonlinear problems. Nevertheless, to the best of our knowledge, this technique has not been employed for inverse design in the field of nonlinear mechanics where multiple solutions exist, especially for the design of morphing and self-deployable structures.

Similar to the inverse design of metasurfaces used in nanophotonics (Liu et al., 2018) or in materials design (Kim et al., 2020; Mao et al., 2020), our paper focuses on problems with multiple design solutions that exist to satisfy equal target properties, such as final shapes and targeted complex motions. We are therefore dealing with a one-to-many mapping problem, where classic feed-forward neural networks become inappropriate as they define the problem as deterministic and make the mapping between the inputs and outputs ambiguous. To address such problems we present a robust inverse-design method that is data-driven and appropriate for designing morphable structures and modeling the complex motions of these structures. We use a GAN-based model (Liu et al., 2018; Arjovsky et al., 2017; Gulrajani et al., 2017) to design morphing structures, that in principle have multiple design solutions for the same target shapes. By taking advantage of the properties of layered composites we find that when bonded, the base (passive) and added (active) layers deform into a prescribed shape due to the strain mismatch induced by the non-homogeneous material properties and/or the (non-homogeneous) actuation. These experimental realizations include materials that can be actuated via different physical principles. Perhaps the most straightforward example is making heat-actuated composites that exploit the mismatch in coefficients of linear thermal expansion in the applied layers, like in bimetallic strips. To test the proposed numerical procedure and explore the parametric space more quickly than via application of heat (and especially cooling), we employ a mechanical analog to thermal actuation that consists of highly flexible sheets of silicone polymer. By carefully stretching the individual active segments and adhering them to the stress-free base layer, the strain mismatch together with the geometric and material properties of each layer determine the curvature of the newly formed structure that forms after the structure is released. We refer to these parameters as the design parameters and they are meant to be determined so that the composite beam can self-deploy into the target shape. We found that this simple toy model can effectively solve many rather complex inverse problems. We used our procedure to design soft actuator beams that morph into target complex shapes during the actuation, potentially leading to the development of a robust method for rapid prototyping and fabricating soft robots, smart-deployable structures and other systems with applicative features.

The remainder of the paper is organized as follows. Section 2 describes the problem and Section 3 the overall description of the GAN-based model, neural network architectures, training dataset creation and details about the training procedure. The description of the composite beam's fabrication is presented in Section 4, while Section 5 discusses the results of the toy model. Section 6 presents the extended use of our approach for designing morphing actuator beams, and the conclusions are drawn in Section 7.

2. Inverse problem of deployable beams

In our system we follow a concept of deployable structures where target final shapes are known and the fabrication parameters are not. By using a flat, thin layer of length L, width W and height H, made of a highly elastic material with a modulus of elasticity E, bonded together with multiple pre-stretched layers that carry finite values of pre-stretch, we ensure the formation of a layered composite beam made of multiple distinct segments that is able to freely deform. The pre-stretched layers can be bonded either on the top or the bottom side, depending on the desired sign of the curvature. The generator network is trained to determine the design parameters $\vec{\boldsymbol{d}}$ that include an amount of pre-stretch λ, length l, width w, height h and modulus of elasticity e of each layer. The amount of pre-stretch is defined as $\lambda = l/l_0$, where l and l_0 are the stretched and initial lengths of each segment, respectively. The details of the system, design parameters and fabrication scheme are presented in Fig. 1.

Note that this model does not strictly represent a morphing structure because the deformation, once it is final, cannot be reversed. However, as the system is elastic it will serve as a toy model to experimentally verify the feasibility of the predicted solution. Exactly the same procedure could be used to design a heat-actuated reversible mechanism that could do mechanical work (movement) when heated or cooled.

3. GAN-based model for inverse design

3.1. Overall description of the model

The generator network is only a part of a larger neural network model consisting of three individual components, see Fig. 2. The first two form a classic GAN model, an unsupervised learning technique consisting of two neural networks, i.e., a generator network and a critic

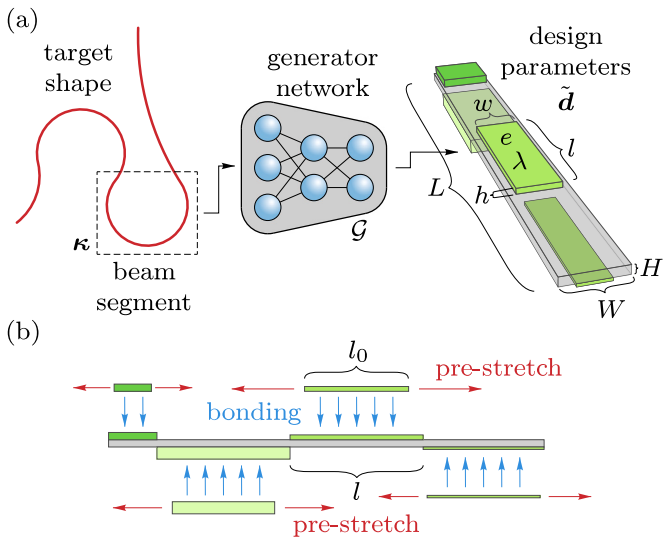

Fig. 1. Neural network-based approach to the inverse design of soft, self-deployable structures. (a) A successfully trained generator network is able to generate candidate solutions of design parameters for forming soft composite beams. The network accepts the target shape representation $\boldsymbol{\kappa}$ for each segment of the beam and outputs the design parameters $\tilde{\boldsymbol{d}} = (l, \lambda, h, w, e)^\intercal$. (b) Individual segments are prepared according to the generated design parameters, i.e., cut to the right dimensions, stretched and bonded to the base layer. Upon release, the composite beam deforms into the target shape.

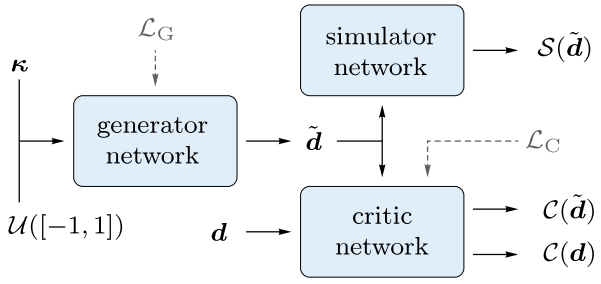

Fig. 2. Individual components of the neural network model for the inverse design of morphing structures. The model consists of three individual networks, the generator and critic networks from the GAN and a pre-trained simulator network. The generator network accepts the target beam-shape representation $\boldsymbol{\kappa}$ concatenated with random noise. Its output, the generated design parameters $\tilde{\boldsymbol{d}}$, are then used as inputs to the critic and simulator networks. The critic network learns from the generated samples $\tilde{\boldsymbol{d}}$ and the samples $\boldsymbol{d}$ from the library of feasible design parameters. Together with the pre-trained simulator network outputting the predicted beam-shape representation $\mathcal{S}(\tilde{\boldsymbol{d}})$, they drive the generator network to generate feasible and accurate design parameters.

network, which compete to create new data with a similar distribution to the training dataset. The generator network is trained to create new data (in our case the design parameters $\tilde{\boldsymbol{d}}$), and the critic network is trained to recognize the authenticity when compared to the given example $\boldsymbol{d}$ from the library of feasible design parameters. In other words, the critic network can be thought of as an agent that assesses the feasibility (e.g., tells the generator network that only geometric properties with non-negative values are desired) of the generated design parameters $\tilde{\boldsymbol{d}}$ and indirectly controls the generator network to produce feasible new data. A pure GAN model is not sufficient to generate accurate design parameters that would result in a target shape of the beam. If the generated design parameters only relied on the critic network, they would eventually produce a deformed shape, but it would probably differ significantly from the target shape. The solution lies in extending the original GAN model with a pre-trained simulator network capable of predicting the shape representation $\mathcal{S}(\tilde{\boldsymbol{d}})$ based on the provided design parameters $\tilde{\boldsymbol{d}}$ (Liu et al., 2018; Kim et al., 2022).

The entire framework for determining the design parameters of the deployable composite beams works as follows: the generator network accepts the target properties in the form of a normalized vector $\boldsymbol{\kappa} = (\kappa, n)^\intercal$ merged with a vector of random noise of size 50 from a uniform distribution $\mathcal{U}([-1,1])$. Thus, an input training example consists of two parameters; the curvature κ of the individual beam segment and n, a discretization number of this segment (all target shapes were discretized with interval of 1 mm). The generator network generates the proposed design parameters $\tilde{\boldsymbol{d}}$, which are then sent to both the critic and simulator networks. The critic network outputs the design feasibility (critic) loss $\mathcal{L}_C$ by predicting the score of the generated sample $C(\tilde{\boldsymbol{d}})$ and the score of the training sample $C(\boldsymbol{d})$ to evaluate the distance between the generated (fake) $\tilde{\boldsymbol{d}}$ and the real sample $\boldsymbol{d}$. In this study, we extended the critic loss by using the gradient penalization (Gulrajani et al., 2017; Petzka et al., 2018),

$$\mathcal{L}_C = C(\tilde{\boldsymbol{d}}) - C(\boldsymbol{d}) + \gamma \left(\max\left(0, \|\nabla C(\hat{\boldsymbol{d}})\|_2 - 1\right)\right)^2, \tag{1}$$

where $\hat{\boldsymbol{d}} = \epsilon \boldsymbol{d} + (1-\epsilon)\tilde{\boldsymbol{d}}$ is the interpolation between the design parameters from the library of feasible design parameters and the generated design parameters, while $\epsilon \sim \mathcal{U}([0,1])$ is a random number and γ is the penalty coefficient. The simulator network predicts the shape representation of the composite beam $\mathcal{S}(\tilde{\boldsymbol{d}})$ for the calculation of the shape loss, which is used with the appropriately set parameter ω for balancing between the feasibility and shape losses to jointly steer the generator network to generate feasible and accurate design parameters $\tilde{\boldsymbol{d}}$,

$$\mathcal{L}_G = -C(\tilde{\boldsymbol{d}}) + \omega \mathrm{MSE}(\boldsymbol{\kappa} - \mathcal{S}(\tilde{\boldsymbol{d}})). \tag{2}$$

Here, MSE represents the mean squared error.

3.2. Neural network architectures

The generator network consists of three sequential dense – batch normalization – ReLU layer blocks with 32 neurons in each dense layer, followed by a dense output layer with 5 neurons having a linear activation function for each of the respective design parameter. The critic network also consists of three sequential dense – leaky ReLU(0.2) layer blocks with 64, 32, and 16 neurons in each dense layer, respectively. The output layer is a dense layer with 1 output neuron having a linear activation function. The architecture of the pre-trained simulator network is similar to the architecture of the inverted generator network and consists of a dense – leaky ReLU(0.1) layer block with 50 neurons and an L2 kernel regularizer with a 0.001 regularization factor. The output layer is a simple dense layer with 2 output neurons and a linear activation function.

3.3. Construction of the training dataset

To train the generator network and the critic network of the GAN-based model, as well as the simulator network, a training dataset was created first. It consists of about 50,000 pairs of design parameters and shape representations. The geometric properties, such as the length l, width w and height h, of active layers were drawn from uniform distributions in the ranges $l \sim \mathcal{U}([20, 200])$ mm, $w \sim \mathcal{U}([10, 20])$ mm, and $h \sim \mathcal{U}([1, 3])$ mm, respectively. The strain-mismatch values were obtained by first sampling the strains ε from a normal distribution with mean 0 and width 0.2 ($\varepsilon \sim \mathcal{N}([0, 0.2])$. Then, 1 was added to all the positive strain values and subtracted from all the negative strain values, according to the relationship $\lambda = \varepsilon + 1 \times \mathrm{sign}(\varepsilon)$, so that $|\lambda| \geq 1$ is forced (note that when $\lambda = 1$ the layer is not strained).

A positive strain mismatch means that the layer must be bonded to the top of the base layer, resulting in positive curvature, and vice versa. The geometric properties of the base layer were fixed at $W = 20$ mm and $H = 2$ mm. In the experiments, both the base and active layers were made of Zhermack Elite Double 32, a two-component, silicone-based elastomer with a modulus of elasticity equal to $E = e = 1.37$ MPa. The

modulus of elasticity was determined by large-displacement cantilever bending tests, see Lolić et al. (2020). To fully construct the training dataset, the curvatures κ needed to be computed. This was done with our in-house-developed code for calculating the curvatures and displacements of layered composite beams. The code was based on the assumptions that the beam is sufficiently thin and not loaded to an extreme degree (e.g., folded) so that the analysis can be limited to small strains, while allowing large rotations and large displacements. This meant that the Euler–Bernoulli beam theory with nonlinear kinematics could be applied. The material (rheological) model was linear elastic, see Lolić et al. (2020). A concise overview of the theory is given in Appendix A and the material alternatives that could be used to replicate the experimental results are given in Appendix C.

3.4. Training

The training samples normalized in $[0, 1]$ were used to train the generator and critic networks. However, for the pre-trained simulator network, the training dataset was identically normalized and split into training, validation and testing datasets in proportions 60, 20, and 20 %, respectively. Here we need to mention that the percentage used for training the simulator network might seem rather low. This is due to the fact that we identified the need for a larger number of training samples to train the generator and critic networks, while the simulator network trained well. Therefore we have expanded the training dataset (from an initial ~37,500 to ~50,000 samples) and wanted to keep the same number of training samples when re-training the simulator network, i.e., roughly 30,000 training pairs. The simulator network was trained first in a classic supervised manner so that it could later be used to help train the generator network. It was compiled using the RMSprop optimizer, a learning rate of $2 \cdot 10^{-5}$, a momentum of 0.9, and the MSE loss function. Training was completed in 30 epochs with 64-sized batches.

Both the generator and critic networks' weights were alternately updated during the training steps using the Adam optimizer with a learning rate of $5 \cdot 10^{-5}$. The parameters γ and ω were set to 10. The generator network was trained in 90,000 generator iterations, while the critic network was trained five times per generator iteration, both with batches of size 64. The plot of negative critic losses is shown in Fig. 3(a), where the simulations of the composite beam's deflections using the generated design parameters during the training procedure are compared for a random training example. A batch of 1,000 randomly selected training samples was used to compute the MSE metric between the target curvatures and the curvatures computed from the generated design parameters at pre-determined iterations, Fig. 3(b). The training procedure was stopped when the metric dropped below $2 \cdot 10^{-5}$, in our case at 90,000 generator iterations. At the end of the training, we also randomly selected 5,000 design parameters from the library of feasible design parameters and generated the same amount to verify the similarity between the density distributions, Fig. 3(c–e). The generator network trained well as it is capable of generating design parameters with a similar distribution to the training dataset for forming beam segments that deform into target shapes.

All the neural networks were trained and developed using the Tensorflow machine learning library running on a laptop computer with 8 GB NVIDIA GeForce RTX 2070 Super graphics card (7.5 compute capability) and NVIDIA CUDA Deep Neural Network Library.

4. Experimental fabrication

We 3D printed four molds of $(180 \times 50 \times h)$ mm in size, where $h \in \{1.0, 1.6, 2.0, 2.4\}$, and an additional mold of size $(300 \times 50 \times 2)$ mm to fabricate the silicone sheets from the aforementioned material. The fabricated sheets were all over-sized in length and width so that the individual segments could be cut according to the generated design parameters. Since the individual active layers were all stretched before being bonded to the base layer of the composite beam, the Poisson effect had to be taken into account. We used $\nu = 0.499$, as measured during the compressibility test of the material. Therefore, each active layer was cut to length l_0 and in width $w/(1 - \nu(\lambda - 1))$, according to the design parameters. We also designed a simple apparatus made of 3D-printed parts and two threaded rods to provide a simple and efficient way to accurately pre-stretch the individual beam segments and position them on the corresponding side of the base layer. A snapshot of the apparatus is shown in Fig. 4(a).

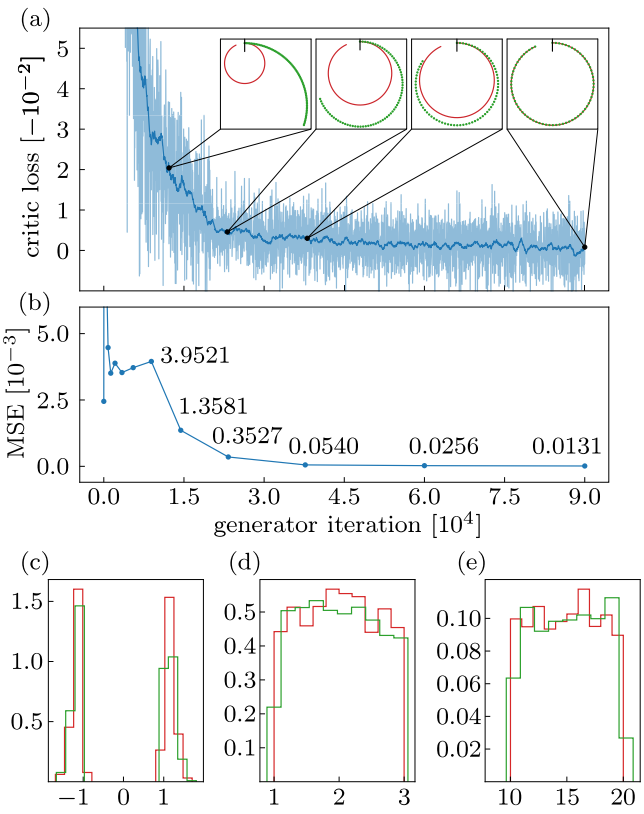

Fig. 3. Training the GAN-based neural network model. (a) Plot of negative critic losses that correlate with the quality of the generated samples. The simulated deflection of a random composite beam (green dots) designed according to the generated design parameters visibly converges to the target shape (red curve). (b) Plot of MSE metric between the target curvatures and the curvatures computed from the 1,000 randomly selected generated design parameters. This metric was computed at pre-determined iterations and used to stop the training procedure when the value dropped below $2 \cdot 10^{-5}$ (c–e) Comparison of density distributions between the training samples (red histograms) and the generated samples (green histograms) for pre-stretches (c), heights (d) and widths (e) of active layers.

In the fabrication procedure, the base layer was first placed on a flat acrylic plate and then the correspondingly cut and pre-stretched beam segment was coated with a thin layer of the same polymer in the liquid phase to achieve practically a perfect bond when positioned on the base layer. An additional acrylic plate and some weights were used to prevent the layers from misaligning, Fig. 4(b). After the bonding material cured, the excess material was removed and the newly formed composite beam was released to deform. This process was repeated in segments to achieve the final shape.

5. Results and discussion

In this section we present and discuss the results of the experiments and simulations on the soft composite beams that deploy into the target shapes. We defined the different shapes that we wanted to fabricate and to verify the algorithms experimentally. We constructed 2 shapes consisting of 3 random samples from the training set, defined

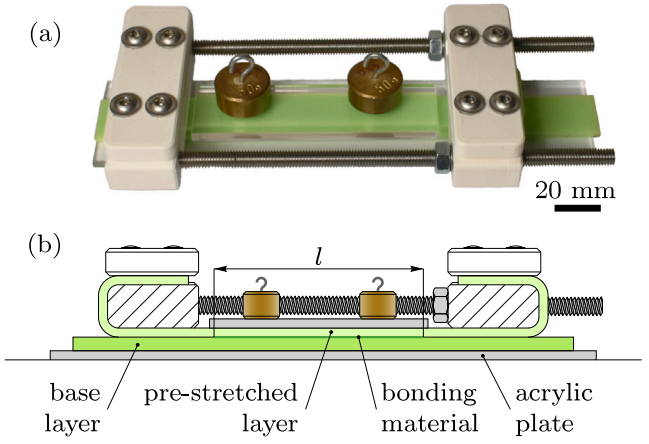

Fig. 4. Apparatus for the fabrication of morphing soft composite beams. (a) Snapshot of the fabrication phase of a composite beam in the apparatus that consists of 3D-printed parts, bolts, nuts and threaded rods. By tightening the nuts, the stretch in individual layers can be controlled very precisely. (b) Cross-sectional view of the fabrication phase. The bonding material is applied to the stretched layer only by the segment length l.

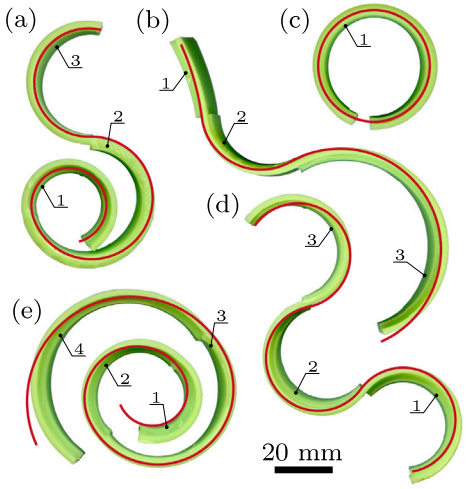

Fig. 5. Comparison of target beam shapes (red curves) and composite beams (green silicone polymer) fabricated according to generated design parameters. (a) and (b) shapes assembled from random training examples, (c) circle, (d) wave, and (e) spiral. The numbers referring to each layer indicate the design parameters used to fabricate each composite beam, see Table 1.

a circular shape and 2 shapes representing a wave and a spiral. All the target shapes are shown with red curves in Fig. 5. The target shapes served as inputs to our trained generator network, which gave us the required design parameters. Since the generator network is able to accept multiple target shapes and therefore generate a number of independent design-parameter candidate solutions, multiple design-parameter combinations were generated for the entire composite beam simultaneously, which allowed us to select the ones that we could actually fabricate. Once all the composite beams were fabricated, each of them was optically scanned using an Epson V550 photo scanner, and the scanned images were processed in Corel Photo-Paint image-editing software (the raw images are shown in Appendix B). The comparison between the target shapes and the fabricated samples is shown in Fig. 5 for the different shapes. The numbers shown in this figure refer to individual segments and serve as identifiers for the design parameters used to fabricate each composite beam. They are gathered in Table 1, which also contains the target radii of curvature and the generated radii of curvature predicted numerically. The generated design parameters were used in our in-house-developed code to calculate the displacements of virtual composite beams. An excellent agreement shows that the generator network is able to successfully generate candidate solutions for design parameters that form soft, deployable composite beams. The last two columns in Table 1 also present a numerical comparison between the radii of curvature for the numerical simulations of the generated design parameters and the measurements from the experiments, but they cannot be directly compared to the target radii of curvature. This is because the radius of curvature of the neutral plane cannot be measured accurately. Therefore, the bonding plane was chosen instead, because it can be easily determined from scanned images of deformed beams.

From Fig. 5(d) and Table 1, case (d), we can see that the generator network has no problem producing different outputs for the same inputs (the target shape of a wave consists of three equal segments), which is not the case when using ordinary neural network architectures. Some deviations also occur due to slightly inaccurate predictions of the design parameters and also due to the fabrication phase. We identified that the layer heights and the pre-stretch amounts have the most influence on the final shapes.

To further test the capabilities of the generator network, we took inspiration from Pablo Picasso's line art. We constructed a shape representing a camel and used a shape representing a handwritten word. By using the generated design parameters to calculate the curvatures and displacements, we were able to closely approximate the target

Table 1
Generated design parameters to fabricate composite beams used in the experiments for (a) and (b) shapes assembled from random training examples, (c) circle, (d) wave, and (e) spiral. Numerical comparison between target r and calculated radii of curvature $\tilde{r}$ of the neutral planes, and numerical comparison between calculated $\tilde{r}_b$ and measured radii of curvature r_b of the bonding planes.

seg.	l [mm]	λ [1]	h [mm]	w [mm]	r [mm]	$\tilde{r}$ [mm]	$\tilde{r}_b$ [mm]	r_b [mm]
$(a)_1$	63	−1.12	1.0	17.9	18.6	18.5	17.3	18.9
$(a)_2$	93	1.14	2.4	19.3	21.1	21.1	19.7	20.2
$(a)_3$	61	1.20	1.6	10.9	12.9	12.7	11.5	14.7
$(b)_1$	26	−1.04	2.4	14.7	88.8	84.5	83.2	73.2
$(b)_2$	40	1.12	1.0	17.1	20.4	20.1	18.8	20.2
$(b)_3$	112	−1.07	1.6	13.3	34.7	35.2	33.9	31.4
$(c)_1$	120	1.13	1.6	18.7	19.2	19.2	17.9	18.8
$(d)_1$	70	−1.15	2.0	14.4	18.0	19.0	17.7	17.6
$(d)_2$	70	1.14	1.6	11.8	18.0	18.0	16.8	17.9
$(d)_3$	70	−1.13	1.0	15.7	18.0	17.7	16.5	17.5
$(e)_1$	38	1.22	2.0	12.4	12.0	12.1	10.9	14.0
$(e)_2$	56	1.14	1.6	10.7	18.0	18.1	16.8	17.3
$(e)_3$	82	1.09	1.0	18.4	26.0	26.0	24.8	24.4
$(e)_4$	112	1.08	2.4	14.0	36.0	36.0	34.7	30.7

shapes. However, some deviations are also visible because the errors are cumulative. For example, incorrect design parameters for the shape of the letter "n" affect the deviations on subsequent letters in the case when the shapes are clamped at one free end. We have also designed a similar target shape to the one that Sun et al. (2022) used in their work (black curves in Fig. 6(c–g)) and generated 10,000 different combinations of design parameters in less than 0.8 s. This is a significantly shorter time compared to the at least 11 min that took to generate only one design in Sun et al. (2022). The reason for this is that we use a different approach for generating the design parameters, which includes the trained generator network, while Sun et al. (2022) used an evolutionary algorithm where a recurrent neural network replaces the finite element method. Also, the mechanics behind the morphing of the beams is not the same. We then randomly selected 5 different design-parameter combinations and plotted the resulting deformed shapes in comparison to the target shapes (dotted curves in Fig. 6(c–g)) where an excellent agreement can be observed, which is not the case in the aforementioned paper. This all indicates that our method is more suitable for the fast and reliable generation of design parameters and the fabrication of morphing structures. To compare the

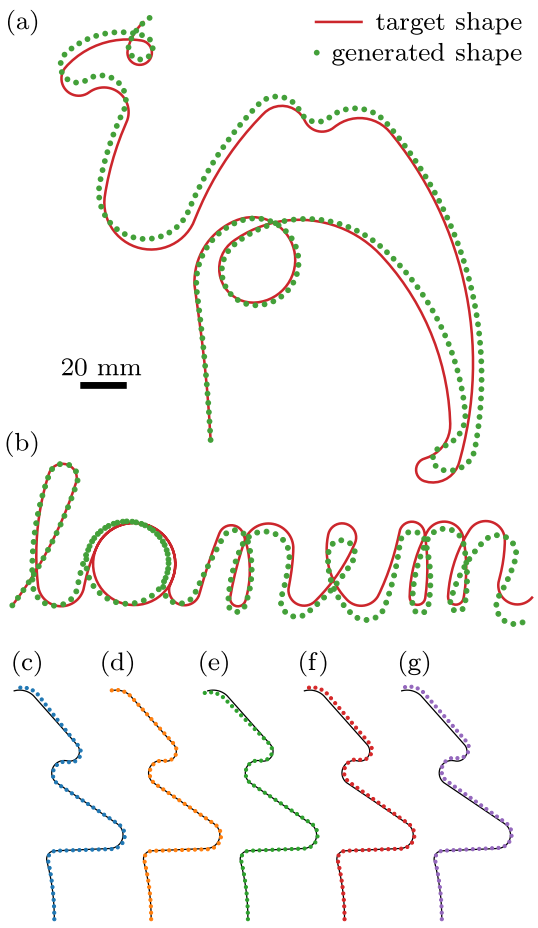

Fig. 6. Generating design parameters for the fabrication of composite beams that deploy into the target shapes, inspired by Pablo Picasso's line art (a) and the handwritten word "lanem" (b). (c-g) Comparison of resulting shapes from different generated design parameters for the target shape, similar to in Sun et al. (2022).

resulting shapes with the target ones, we also computed the root-mean-square errors between the calculated curvatures from the generated design parameters and the target curvatures for each subfigure in Fig. 6. The values are $\{1.43, 6.47, 0.78, 0.76, 0.65, 0.67, 1.01\}\cdot 10^{-3}$ 1/mm for each case in Fig. 6, respectively.

6. Morphing composite beams

So far we have shown how GAN-based architectures can be successfully used for the inverse design of the mechanical analog of morphing structures. In this section we increase the complexity of the inverse design and include target complex motions during the actuation with temperature. In this numerical example we replaced the pre-stretch parameter λ with the coefficient of linear thermal expansion α and the temperature load ΔT according to the relation $\lambda - 1 = -\alpha\Delta T$. Previously, a positive pre-stretch meant that the active layer needed to be bonded to the top side of the base layer, resulting in a positive curvature. Now, to achieve the same effect, an active layer can either be placed on the top side and cooled down (negative ΔT) or on the bottom side and heated up (positive ΔT). We kept the same geometric properties of active layers as before, and the material properties were $\alpha \sim \mathcal{U}([0.001, 0.009])$ 1/K and $e \sim \mathcal{U}([1, 2])$ MPa, while the temperature load was $\Delta T \sim \mathcal{U}([-100, 100])$ K. The properties of the base layer were the same, except for the coefficient of linear thermal expansion, which was set to 0 to maintain similarity with the mechanical analog. The neural network architecture was just slightly modified, increasing the number of neurons in the generator network's output layer to 6. This is because the design-parameter space now carries 6 independent variables (we added ΔT and replaced λ with α).

Table 2
Generated design parameters for forming soft morphing beams that demonstrate complex target motions during the actuation with temperature.

seg.	l [mm]	h [mm]	w [mm]	e [MPa]	α [1/K]
$(a)_1$	17	2.6	17.6	1.47	0.0048
$(a)_2$	81	2.2	17.6	1.42	0.0042
$(b)_1$	44	2.9	10.6	1.65	0.0024
$(b)_2$	64	2.6	12.0	1.96	0.0028
$(b)_3$	64	2.1	12.5	1.80	0.0018

To design a morphing composite beam we first constructed two target shapes that the actuator has to include in its motion, e.g., the home position and the end position. Then, a large number of candidate design parameters were generated and the appropriate solution was chosen using a simple algorithm implementing the following conditions: geometric and material properties of the morphing composite beam have to be segment-wise equal for both target shapes. However, they are allowed to differ between individual segments, and the temperature load ΔT had to be equal for all those segments as the whole beam was being heated/cooled. These conditions gave us two solutions for the design parameters (for both target shapes) with negligible differences for the geometric and material properties due to the large number of generated design parameters to choose from.

To showcase the extended capabilities of our toy model we present the designs of two different morphing composite beams that can be actuated by temperature to carry out a complex prescribed motion. Fig. 7(a) shows the first beam configuration that is able to morph from the target home position (dashed red curve) when cooled down by 25 K, and into the target end position (solid red curve) when heated by 35 K from the initial temperature. Similarly, the second beam configuration shown in Fig. 7(b) can make a continuous movement between the target home and end positions when heated continuously by 51 K. A good match is obtained between the target and algorithmically modeled configurations. Nevertheless, we should mention that an exact match could not be obtained due to the aforementioned condition of selecting the design parameter solution. The generated design parameters are listed in Table 2 and are referred to layers indicated by numbers in respective insets in Figs. 7(a) and (b) that correspond to composite beams presented in this figure.

7. Conclusions

We presented a method for forming soft composite beams that can morph into target shapes. First, the inverse problem and the toy model are described. The problem is defined as a self-deployable composite beam where the target shape is known, but the design parameters for forming individual segments are not. The composite beam is made of a load-free base layer to which a number of pre-stretched layers are bonded according to the design parameters. To solve this problem we adopted a machine learning approach that employs a generative modeling technique. Specifically, we developed a neural network architecture consisting of three neural networks: the generator network, the critic network and the pre-trained simulator network. The generator network tries to generate candidate solutions for the design parameters, while the critic network ensures the feasibility of the generated design parameters, and the simulator network verifies their accuracy. In addition, we developed a simple apparatus that enables the straightforward fabrication of composite beams. For the experiments, we defined several target shapes, generated design parameters, and fabricated composite beams.

The comparison between the target and fabricated shapes showed excellent agreement with only minimal deviations between the target and calculated radii of curvature from the generated design parameters.

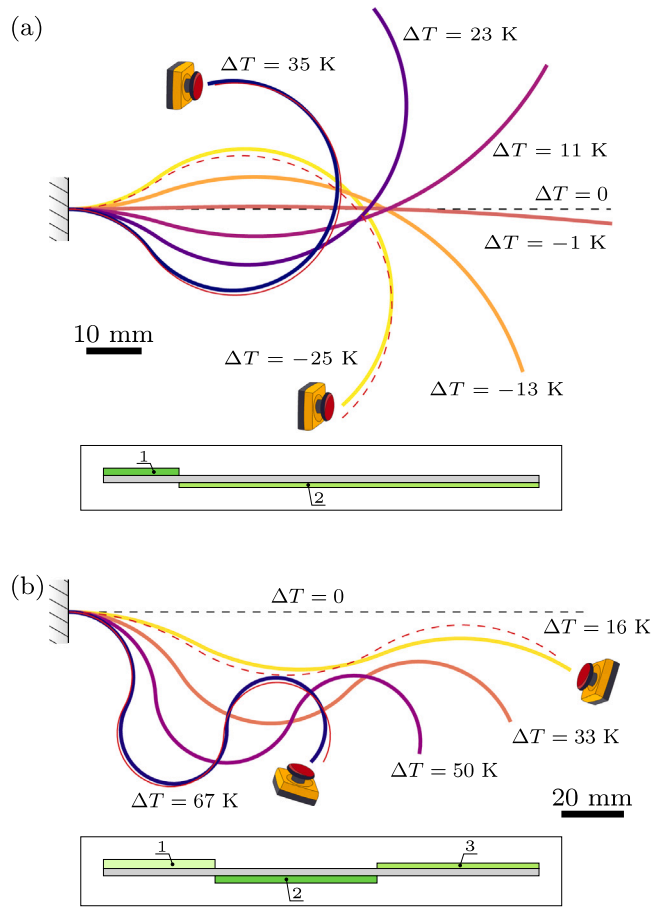

Fig. 7. Generating design parameters for the fabrication of soft morphing beams that can be actuated by heating/cooling to demonstrate a complex motion. Two examples of beams (a) and (b) that morph from the target home positions (dashed red curves) into the target end positions (solid red curves). The dashed black lines represent the initial shapes of both beams, which are (a) 98 mm and (b) 172 mm long. The respective insets in (a) and (b) show the structure of morphing beams with the design parameters given in Table 2.

However, slightly larger deviations were found when comparing the calculated radii of curvature from the generated design parameters and the measured radii of curvature for the actual fabricated beams. This was mainly due to experimental errors, such as the lack of precision during the cutting stage, incomplete bonds between layers, and measuring errors. However, as observed from the numerical experiments, forming composite beams with a larger number of segments presents a moderate difficulty because any possible errors in the first segments can break the agreement between the target and actual shapes. We also compared our approach with the work of Sun et al. (2022), where we constructed a similar shape as they did, generated the design parameters and compared the simulated shapes with the target ones. We found that our approach is not only faster, but also more accurate at generating the design parameters in this particular case. However, we need to mention that their neural-network-empowered evolutionary algorithm still holds great potential for solving inverse problems. The ideas from the toy model were then used to design soft morphing composite beams that, when actuated with temperature, can exhibit complex target motions. This was demonstrated with two numerical showcases, resembling a soft-robot actuator.

The presented method demonstrated its potential for designing morphing structures that have the ability to morph into target shapes. It was shown that when using the strain mismatch as the potential energy storage, no additional external stimulus or activation energy is required

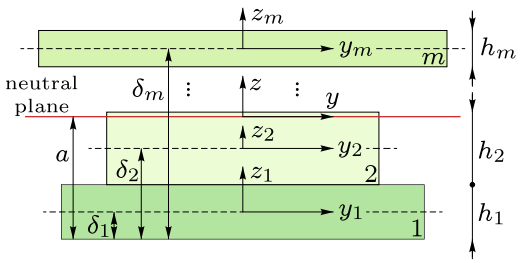

Fig. A.8. Cross-section of an m-layered composite beam and the corresponding coordinate systems.

to transform the structure from an initial to a deformed configuration. We also showed how simple models are able to solve more complex inverse problems compared to our toy model. We believe that combining the capabilities of the presented method and the advantages of such structures holds great potential for developing advanced morphing structures and will motivate further studies.

CRediT authorship contribution statement

Tomaž Brzin: Conceptualization, Data curation, Formal analysis, Investigation, Methodology, Software, Writing – original draft, Writing – review & editing. **Miha Brojan:** Conceptualization, Funding acquisition, Investigation, Methodology, Project administration, Resources, Supervision, Writing – original draft, Writing – review & editing.

Declaration of competing interest

The authors declare that they have no known competing financial interests or personal relationships that could have appeared to influence the work reported in this paper.

Data availability

Data will be made available on request.

Acknowledgment

T.B. and M.B. gratefully acknowledge the financial support of the Slovenian Research Agency.

Funding

This work was supported by the Slovenian Research Agency under Grants J2-2499 and J2-4449.

Appendix A. Theory of layered composite beams

In the following lines, some of the basics of strain-mismatched composite beams are presented (see also, e.g., Timoshenko (1925)).

Fig. A.8 presents the rectangular cross-section of an m-layered composite beam, where each layer has width w_i and height h_i, while it is made of a material with a modulus of elasticity e_i, $i \in \{1, \dots, m\}$. On each layer we define a local coordinate system (y_i, z_i) that is offset by $-a + \delta_i$ from the main material coordinate system (y, z). Each layer is pre-stretched by λ_i.

The main material coordinate system (y, z) lies on the neutral plane with its origin positioned at the mid-width and distanced by a from the bottom of the beam. At each cross-section a curvature κ is recorded. Due to the pre-stretch of individual layers, stress σ_i occurs in each layer, according to the following expression

$$\sigma_i(z) = e_i(-z\kappa + \lambda_i - 1). \tag{A.1}$$

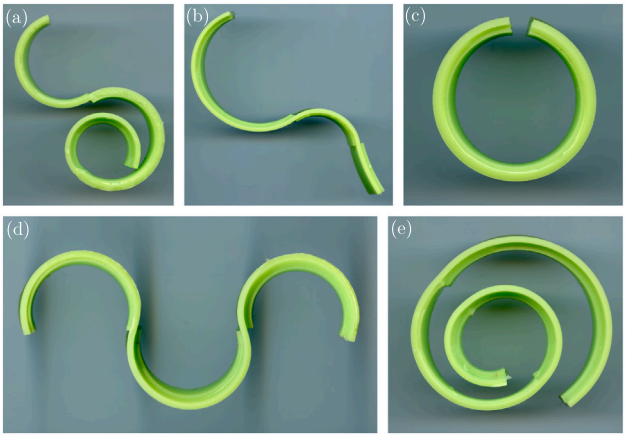

Fig. B.9. Screenshots of the raw images from the experiments.

It follows from the free boundary conditions that the inner axial force and the inner bending moment have to be equal to zero,

$$\sum_{i=1}^{m} w_i \int_z \sigma_i(z)\mathrm{d}z = 0, \tag{A.2}$$

$$\sum_{i=1}^{m} w_i \int_z \sigma_i(z) z\mathrm{d}z = 0. \tag{A.3}$$

Introducing Eq. (A.1) into Eqs. (A.2) and (A.3) and transforming to local coordinate systems with $z = -a + \delta_i + z_i$ we can obtain the following system of equations,

$$\begin{gathered} \sum_{i=1}^{m} A_i e_i \left((a-\delta_i)\kappa + \lambda_i - 1\right) = 0, \\ \sum_{i=1}^{m} \left[A_i e_i (a-\delta_i)((a-\delta_i)\kappa + \lambda_i - 1) + e_i I_i \kappa\right] = 0, \end{gathered} \tag{A.4}$$

where $A_i = w_i h_i$ and $I_i = w_i h_i^3/12$. The solution for our case study with $m = 2$, gives the expression for calculating κ, see Timoshenko (1925),

$$\kappa = \mathrm{sign}(\lambda) \frac{6hHwW(h+H)(\mathrm{abs}(\lambda)-1)}{(wh^2 - WH^2)^2 + 4hHwW(h+H)^2}. \tag{A.5}$$

With a known curvature κ, it is straightforward to calculate displacements from the known expressions from differential geometry:

$$\vartheta'(s) = \kappa(s), \quad x'(s) = \cos\vartheta(s), \quad z'(s) = \sin\vartheta(s), \tag{A.6}$$

where s is the curvilinear coordinate along the longitudinal axis of the beam. The boundary conditions are

$$\vartheta(0) = 0, \quad x(0) = 0, \quad z(0) = 0. \tag{A.7}$$

Appendix B. Raw images of the experimental samples

The raw versions of the experimental samples from Fig. 5 are given in Fig. B.9.

Appendix C. Alternative materials

Here, we briefly discuss the materials that we have tested during the experimental stage and the materials that could also be used as alternatives in replicating our experiments.

- **VPS (a-silicone) duplicating materials**: In our experiments we used Zhermack Elite Double 32, a two-component silicone-based elastomer. This family of materials is primarily used in the dental sector for the purpose of duplication (www.zhermack.com). A series of tests were performed on the whole family of the product ranging from Elite Double 8 (the softest version) to Elite Double 32 (the stiffest version that is approximately 5 times stiffer than the softest one). We found the latter version is the most appropriate for conducting our experiments. Moreover, we recommend using the standard versions, not the "fast-curing" ones that demand (too) fast assembly of the composites, and highly recommend using a professional mixer for mixing the catalyst and the base to avoid trapping air bubbles.
- **VHB sealing tapes**: Our initial tests on composite beams were made using a very-high-bond (VHB) self-adhesive sealing tapes from 3M (www.3m.com). They are quite easy to work with, however in our case we found that the adherence was not sufficient when joining two pieces of the same material together.
- **3D printing TPU materials**: The development of very soft 3D printing materials offers a great potential for fabricating composite beams and beyond, because individual pieces can be simply 3D-printed into the desired forms. Additionally, such approach has an important advantage since no cutting is needed in the process of the fabrication. We recommend a commercially available Recreus Filaflex 60 A Pro filament (www.recreus.com). However, the non-homogeneity of the printed composite layer could cause some unwanted warpings after the release of the composite from the stretching apparatus.

References

Arjovsky, M., Chintala, S., Bottou, L., 2017. Wasserstein generative adversarial networks. In: Precup, D., Teh, Y.W. (Eds.), Proceedings of the 34th International Conference on Machine Learning. In: Proceedings of Machine Learning Research, vol. 70, pp. 214–223.

Battista, D., Curatolo, M., Nardinocchi, P., 2019. Swelling-induced eversion and flattening in naturally curved gel beams. Int. J. Mech. Sci. 161–162, 105071. http://dx.doi.org/10.1016/j.ijmecsci.2019.105071.

Cang, R., Li, H., Yao, H., Jiao, Y., Ren, Y., 2018. Improving direct physical properties prediction of heterogeneous materials from imaging data via convolutional neural network and a morphology-aware generative model. Comput. Mater. Sci. 150, 212–221. http://dx.doi.org/10.1016/j.commatsci.2018.03.074.

Caruso, N., Cvetković, A., Lucantonio, A., Noselli, G., DeSimone, A., 2018. Spontaneous morphing of equibiaxially pre-stretched elastic bilayers: The role of sample geometry. Int. J. Mech. Sci. 149, 481–486. http://dx.doi.org/10.1016/j.ijmecsci.2017.08.049.

Choi, G.P.T., Dudte, L.H., Mahadevan, L., 2019. Programming shape using kirigami tessellations. Nature Mater. 18, 999–1004. http://dx.doi.org/10.1038/s41563-019-0452-y.

Dang, X., Feng, F., Plucinsky, P., James, R.D., Duan, H., Wang, J., 2022. Inverse design of deployable origami structures that approximate a general surface. Int. J. Solids Struct. 234–235, 111224. http://dx.doi.org/10.1016/j.ijsolstr.2021.111224.

DeSimone, A., 2018. Spontaneous bending of pre-stretched bilayers. Meccanica 53 (3), 511–518. http://dx.doi.org/10.1007/s11012-017-0732-z.

Ding, Z., Weeger, O., Qi, H.J., Dunn, M.L., 2018. 4D rods: 3D structures via programmable 1D composite rods. Mater. Des. 137, 256–265. http://dx.doi.org/10.1016/j.matdes.2017.10.004.

Ding, Z., Yuan, C., Peng, X., Wang, T., Qi, H.J., Dunn, M.L., 2017. Direct 4D printing via active composite materials. Sci. Adv. 3 (4), e1602890. http://dx.doi.org/10.1126/sciadv.1602890.

Gulrajani, I., Ahmed, F., Arjovsky, M., Dumoulin, V., Courville, A., 2017. Improved training of Wasserstein GANs. In: Guyon, I., von Luxburg, U., Bengio, S., Wallach, H., Fergus, R., Vishwanathan, S., Garnett, R. (Eds.), Proceedings of the 31st International Conference on Neural Information Processing Systems. In: Advances in Neural Information Processing Systems, vol. 31, pp. 5769–5779.

Guo, W., Li, M., Zhou, J., 2013. Modeling programmable deformation of self-folding all-polymer structures with temperature-sensitive hydrogels. Smart Mater. Struct. 22 (11), 115028. http://dx.doi.org/10.1088/0964-1726/22/11/115028.

Guo, Q., Pan, Y., Lin, J., Wan, G., Xu, B., Hua, N., Zheng, C., Huang, Y., Mei, Y., Chen, W., Chen, Z., 2020. Programmable 3D self-folding structures with strain engineering. Adv. Intell. Syst. 2 (12), 2000101. http://dx.doi.org/10.1002/aisy.202070121.

Guo, K., Yang, Z., Yu, C.-H., Buehler, M.J., 2021. Artificial intelligence and machine learning in design of mechanical materials. Mater. Horiz. 8 (4), 1153–1172. http://dx.doi.org/10.1039/D0MH01451F.

Holmes, D.P., 2019. Elasticity and stability of shape-shifting structures. Curr. Opin. Colloid & Interface Sci. 40, 118–137. http://dx.doi.org/10.1016/j.cocis.2019.02.008.

Huo, Z., He, J., Pu, H., Luo, J., Li, D., 2022. Design and printing of embedded conductive patterns in liquid crystal elastomer for programmable electrothermal actuation. Virtual Phys. Prototyp. 17 (4), 881–893. http://dx.doi.org/10.1080/17452759.2022.2087096.

Ionov, L., 2015. Polymeric actuators. Langmuir 31 (18), 5015–5024. http://dx.doi.org/10.1021/la503407z.

Kapsalyamov, A., Hussain, S., Brown, N.A.T., Goecke, R., Hayat, M., Jamwal, P.K., 2023. Synthesis of a six-bar mechanism for generating knee and ankle motion trajectories using deep generative neural network. Eng. Appl. Artif. Intell. 117, 105500. http://dx.doi.org/10.1016/j.engappai.2022.105500.

Kim, W., Kim, S., Lee, M., Seok, J., 2022. Inverse design of nanophotonic devices using generative adversarial networks. Eng. Appl. Artif. Intell. 115, 105259. http://dx.doi.org/10.1016/j.engappai.2022.105259.

Kim, B., Lee, S., Kim, J., 2020. Inverse design of porous materials using artificial neural networks. Sci. Adv. 6 (1), eaax9324. http://dx.doi.org/10.1126/sciadv.aax9324.

Liu, Z., Zhu, D., Rodrigues, S.P., Lee, K.T., Cai, W., 2018. Generative model for the inverse design of metasurfaces. Nano Lett. 18 (10), 6570–6576. http://dx.doi.org/10.1021/acs.nanolett.8b03171.

Lolić, D., Zupan, D., Brojan, M., 2020. A consistent finite element formulation for laminated composites with nonlinear interlaminar constitutive law. Compos. Struct. 247, 112445. http://dx.doi.org/10.1016/j.compstruct.2020.112445.

Ma, L., Mungekar, M., Roychowdhury, V., Jawed, M.K., 2023. Rapid design of fully soft deployable structures via kirigami cuts and active learning. URL: https://arxiv.org/abs/2303.11295.

Mao, Y., He, Q., Zhao, X., 2020. Designing complex architectured materials with generative adversarial networks. Sci. Adv. 6 (17), eaaz4169. http://dx.doi.org/10.1126/sciadv.aaz4169.

Nojoomi, A., Jeon, J., Yum, K., 2021. 2D material programming for 3D shaping. Nature Commun. 12 (1), 603. http://dx.doi.org/10.1038/s41467-021-20934-w.

Petzka, H., Fischer, A., Lukovnikov, D., 2018. On the regularization of Wasserstein GANs. URL: https://arxiv.org/abs/1709.08894.

Pezzulla, M., Shillig, S.A., Nardinocchi, P., Holmes, D.P., 2015. Morphing of geometric composites via residual swelling. Soft Matter 11 (29), 5812–5820. http://dx.doi.org/10.1039/c5sm00863h.

Qiu, W., Xu, Y., Xu, F., Huo, Y., 2023. Programmable electric-field-induced bending shapes of dielectric liquid crystal elastomer sheets. Extreme Mech. Lett. 60, 101982. http://dx.doi.org/10.1016/j.eml.2023.101982.

Regenwetter, L., Nobari, A.H., Ahmed, F., 2022. Deep generative models in engineering: A review. J. Mech. Des. 144 (7), 071704. http://dx.doi.org/10.1115/1.4053859.

Siéfert, E., Reyssat, E., Bico, J., Roman, B., 2019. Bio-inspired pneumatic shape-morphing elastomers. Nature Mater. 18 (1), 24–29. http://dx.doi.org/10.1038/s41563-018-0219-x.

Sun, X., Yue, L., Yu, L., Shao, H., Peng, X., Zhou, K., Demoly, F., Zhao, R., Qi, H.J., 2022. Machine learning-evolutionary algorithm enabled design for 4D-printed active composite structures. Adv. Funct. Mater. 32 (10), 2109805. http://dx.doi.org/10.1002/adfm.202109805.

Timoshenko, S.P., 1925. Analysis of bi-metal thermostats. J. Opt. Soc. Am. Rev. Sci. Instrum. 11 (3), 233–255. http://dx.doi.org/10.1364/JOSA.11.000233.

van Manen, T., Janbaz, S., Zadpoor, A.A., 2018. Programming the shape-shifting of flat soft matter. Mater. Today 21 (2), 144–163. http://dx.doi.org/10.1016/j.mattod.2017.08.026.

Wang, J., Zhang, B., Lei, P., Dai, N., 2019. Photo-induced bending and buckling of polymer sheets. In: IOP Conference Series - Materials Science and Engineering, vol. 493, 012029. http://dx.doi.org/10.1088/1757-899X/493/1/012029.

Wu, Y., Hao, X., Xiao, R., Lin, J., Wu, Z.L., Yin, J., Qian, J., 2019. Controllable bending of bi-hydrogel strips with differential swelling. Acta Mech. Solida Sin. 32 (5), 652–662. http://dx.doi.org/10.1007/s10338-019-00106-6.

Wu, L., Liu, L., Wang, Y., Zhai, Z., Zhuang, H., Krishnaraju, D., Wang, Q., Jiang, H., 2020. A machine learning-based method to design modular metamaterials. Extreme Mech. Lett. 36, 100657. http://dx.doi.org/10.1016/j.eml.2020.100657.

Yonekura, K., Wada, K., Suzuki, K., 2022. Generating various airfoils with required lift coefficient by combining NACA and Joukowski airfoils using conditional variational autoencoders. Eng. Appl. Artif. Intell. 108, 104560. http://dx.doi.org/10.1016/j.engappai.2021.104560.

Zavodnik, J., Wang, Y., Yan, W., Brojan, M., Jawed, M.K., 2023. Soft kirigami composites for form-finding of fully flexible deployables. URL: https://arxiv.org/abs/2301.06597.